A weakly coupled semiconductor superlattice as a harmonic hypersonic-electrical transducer

2015 New J. Phys. 17 083064

(http://iopscience.iop.org/1367-2630/17/8/083064)

New Journal of Physics
The open access journal at the forefront of physics

Deutsche Physikalische Gesellschaft DPG
IOP Institute of Physics

Published in partnership with: Deutsche Physikalische Gesellschaft and the Institute of Physics

OPEN ACCESS

RECEIVED
28 May 2015

REVISED
11 July 2015

ACCEPTED FOR PUBLICATION
13 July 2015

PUBLISHED
1 September 2015

PAPER

A weakly coupled semiconductor superlattice as a harmonic hypersonic-electrical transducer

C L Poyser[1], A V Akimov[1], A G Balanov[2], R P Campion[1] and A J Kent[1]

[1] School of Physics and Astronomy, University of Nottingham, University Park, Nottingham, NG7 2RD, UK
[2] Department of Physics, Loughborough University, Loughborough, LE11 3TU, UK

E-mail: caroline.poyser@nottingham.ac.uk

Keywords: coherent phonons, superlattices, electron transport, high frequency, acoustics

Abstract

We study experimentally and theoretically the effects of high-frequency strain pulse trains on the charge transport in a weakly coupled semiconductor superlattice. In a frequency range of the order of 100 GHz such excitation may be considered as single harmonic hypersonic excitation. While travelling along the axis of the SL, the hypersonic acoustic wavepacket affects the electron tunnelling, and thus governs the electrical current through the device. We reveal how the change of current depends on the parameters of the hypersonic excitation and on the bias applied to the superlattice. We have found that the changes in the transport properties of the superlattices caused by the acoustic excitation can be largely explained using the current–voltage relation of the unperturbed system. Our experimental measurements show multiple peaks in the dependence of the transferred charge on the repetition rate of the strain pulses in the train. We demonstrate that these resonances can be understood in terms of the spectrum of the applied acoustic perturbation after taking into account the multiple reflections in the metal film serving as a generator of hypersonic excitation. Our findings suggest an application of the semiconductor superlattice as a hypersonic-electrical transducer, which can be used in various microwave devices.

1. Introduction

Since the pioneering work of Esaki and Tsu [1], semiconductor superlattices (SLs) have attracted very large interest owing to their vertical transport properties and potential applications at microwave frequencies [2–6]. During the past decade, studies of the interaction of carriers with high-frequency electrical and far infrared fields in SLs have been intensively carried out, and as a result, a number of phenomena have been revealed, including: Bloch gain [7–10]; quantum cascade lasing [11, 12]; parametric THz radiation [13, 14]; noise-induced current switching [15]; coherence resonance [16, 17]; and high-frequency quasi-periodic and chaos generation [18–22]. In addition, new devices with prospective applications in microwave and THz technologies have been developed, e.g. superlattice millimeter wave mixers [23], frequency multipliers [24] and random number generators [25]. In parallel with electrical and optical studies, the interaction of carriers in the SLs with gigahertz (GHz) and terahertz (THz) phonons (i.e. hypersound) has been studied in a number of works, experimentally [26] and theoretically [27]. This has led to the development of a sound amplification by stimulated emission of radiation device [28] and electrical control of hypersound fluxes in phononic chips [29, 30]. From these earlier studies it is clear that hypersound has the ability to control carrier transport, and thus to control the electrical and microwave responses in the SLs. In other words, carriers, due to their efficient interaction with phonons, may play a role of a transducer between sound and high-frequency (up to THz) electric field in the semiconductor SLs. Recent theoretical studies of the interaction of harmonic hypersound with carriers in SLs [31, 32] have shown interesting new phenomena. In particular, it was found that a high-frequency acoustic wave can induce different types of single electron oscillations with a frequency several orders of magnitude higher than that of the acoustic wave itself [31].

The main challenge of the experiments in this field is the generation of high-amplitude coherent GHz and THz acoustic waves with a spectrum close to the monochromatic [33–36]. Indeed, there are well developed methods of picosecond acoustics allowing manipulation of high-amplitude strain pulses, but the acoustic wave packet in this case possesses a broad spectrum [37]. The most appropriate technique for the search of harmonic hypersonic-electrical phenomena in SLs is to use multiple periodic strain pulses generated by the train of optical pulses from a regeneratively amplified femtosecond laser. This technique is, in many cases, suitable for generation of high-amplitude harmonic hypersound and was used earlier for experiments such as the generation of shear waves in liquids [38] and measuring acoustic attenuation in vitreous silica [39]. However this method has not yet been exploited for studies of electrical properties in semiconductor SLs.

The aim of the present work is to apply a periodic train of strain pulses with a frequency 10–100 GHz to a semiconductor SL and study the effect of harmonic hypersound waves on the vertical electron current. Based on the experimental observations we develop a theoretical approach which describes hypersonic-electrical transduction in the semiconductor SLs. As the experimental structure we take an n-doped ($\sim 10^{17}\mathrm{cm}^{-3}$) SL which contains GaAs quantum wells (QWs) with rather thick AlAs barriers that allow us to consider the QW carrier states as weakly coupled. In such a SL sequential tunnelling dominates over miniband transport [40]. We observe a considerable (up to 3 %) decrease of the SL current induced by the hypersonic waves which shows that the semiconductor SL can serve as an efficient hypersonic-electrical transducer. For theoretical analysis we use the phenomenological approach previously applied to the study of electromagnetic waves in SLs, and get a good agreement between the experiment and theory for the impact of harmonic hypersonic excitation on the SL electrical current. Finally, we use the same experimental technique, and results of the theoretical studies, for the analysis of the frequency dependence of the amplitude of quasi-monochromatic hypersonic waves emitted into the GaAs substrate from Al thin films prepared in different ways and excited by a train of femtosecond optical pulses. In the summary we discuss the prospective of exploiting SLs as hypersonic-electrical transducers in the microwave and THz ranges.

2. Experiment

2.1. Samples and experimental technique

The scheme of the studied sample, which was grown on a 0.164 mm-thick semi-insulating GaAs substrate by molecular beam epitaxy, is shown in figure 1 (a). The SL consists of 50 periods of GaAs and AlAs layers with thicknesses 5.9 and 3.9 nm respectively, n-doped with Si ($\sim 10^{17}\mathrm{cm}^{-3}$). The n^{+}–GaAs layers at each end of the SL play the role of contacts for vertical transport measurements and 20.2 nm GaAs spacer layers with gradient doping were grown to screen the SL structure from the higher doping of the contacts. The structures were prepared in the form of mesas with various diameters (from 50 up to 400 μm), and the results presented here were obtained using the mesas with diameter 100 μm. The current–voltage characteristics measured at the temperature, $T = 5$ K which was used throughout these experiments, are shown in figure 1 (b) for 7 mesas (denoted M1–M7) of the same design. All mesas demonstrate current–voltage characteristics typical of GaAs/AlAs SLs studied in previous works [30, 41]. The dash–dot–dot vertical lines indicate the values of the threshold voltages, V_t, above which the space charge and negative conductivity effects become apparent for mesa M2. It can be seen in figure 1 (b) that the current–voltage characteristics of all the mesas are very similar to each other.

On the face of the GaAs substrate opposite to the SL, Al films with various thicknesses, ξ, (from 30 up to 150 nm) were deposited (see figure 1 (a)). The film plays the role of optoacoustic transducer: the excitation of the Al film by optical pulses from a femtosecond laser results in the injection of picosecond strain pulses into the GaAs substrate [37]. The duration of the strain pulses is in the range 5–15 ps, and depends mainly on the thickness of the Al film used. In our experiments we use a regeneratively amplified Ti:Sapphire laser which produces 100 fs optical pulses with a 5 kHz repetition rate and energy 0.5 mJ. The scheme of the excitation and electrical detection of the hypersonic impact on the vertical current in the SL is shown in figure 1 (c). The essential part of the experimental arrangement is the Fabry–Perot (FP) cavity which transforms a single optical pulse from the laser into a train of optical pulses with the period, f^{-1}, defined by the distance between the mirrors of FP cavity. The train of optical pulses is focused on the Al film to a spot with an approximate diameter of 100 μm, which results in the injection of the corresponding train of picosecond strain pulses into the GaAs substrate.

Figure 2 (a) shows an numerical simulation of an individual strain pulse such as would be expected from the excitation of a 30 nm Al film [37, 42], and figure 2 (b) shows the train of strain pulses with the repetition rate $f =$ 50 GHz. For simplicity, in the simulations shown in figure 2 we have assumed zero acoustic mismatch between Al film and GaAs. The simulations for various mismatches will be discussed in section 3.2 of the present paper. The pulses in the train are decaying in accordance with the reflectivity values of the FP cavity (97% and 92% for input and output mirrors respectively). Figure 2 (c) shows the power spectral density $S_f(\nu)$ of strain pulse trains

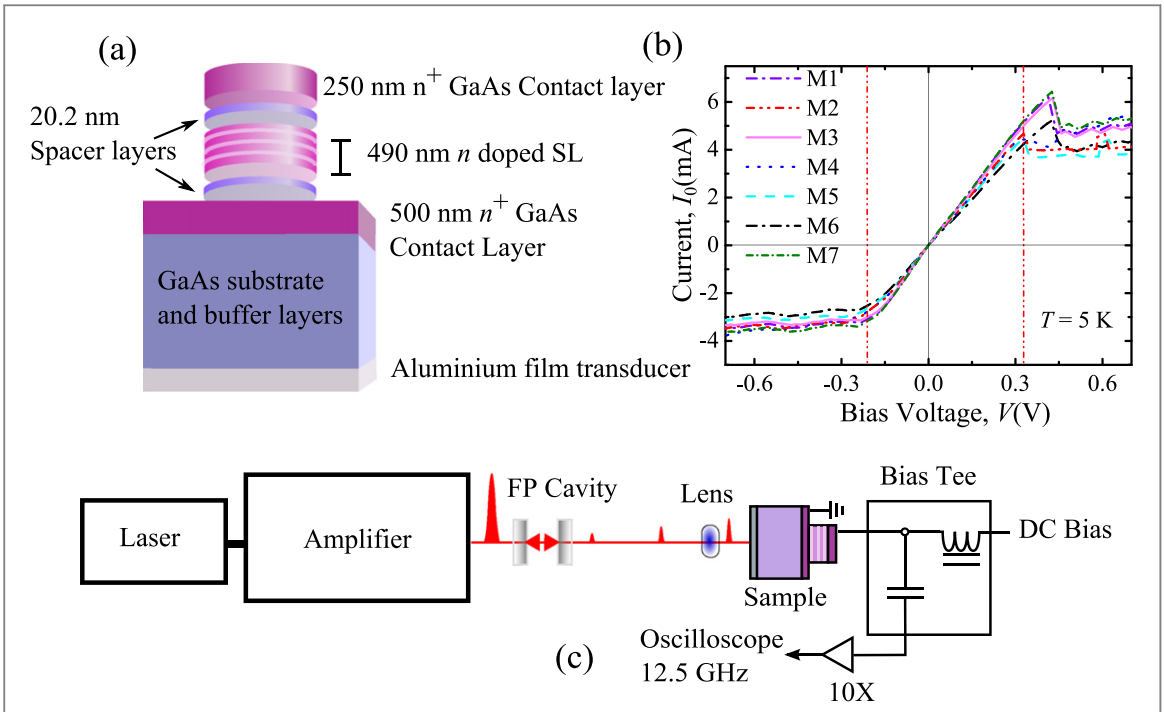

Figure 1. (a) The sample structure which includes the weakly coupled superlattice (SL), contacts and spacer layers; the optoelastic Al film transducer is deposited on the side of the GaAs substrate opposite to the device. (b) Current–voltage characteristics of seven different mesas M1–M7 studied in the experiments. (c) Experimental arrangement for measuring the electrical response from the train of the picosecond pulses in the SL; FP is an optical Fabry–Pérot cavity for the transformation of a single strain pulse to a train.

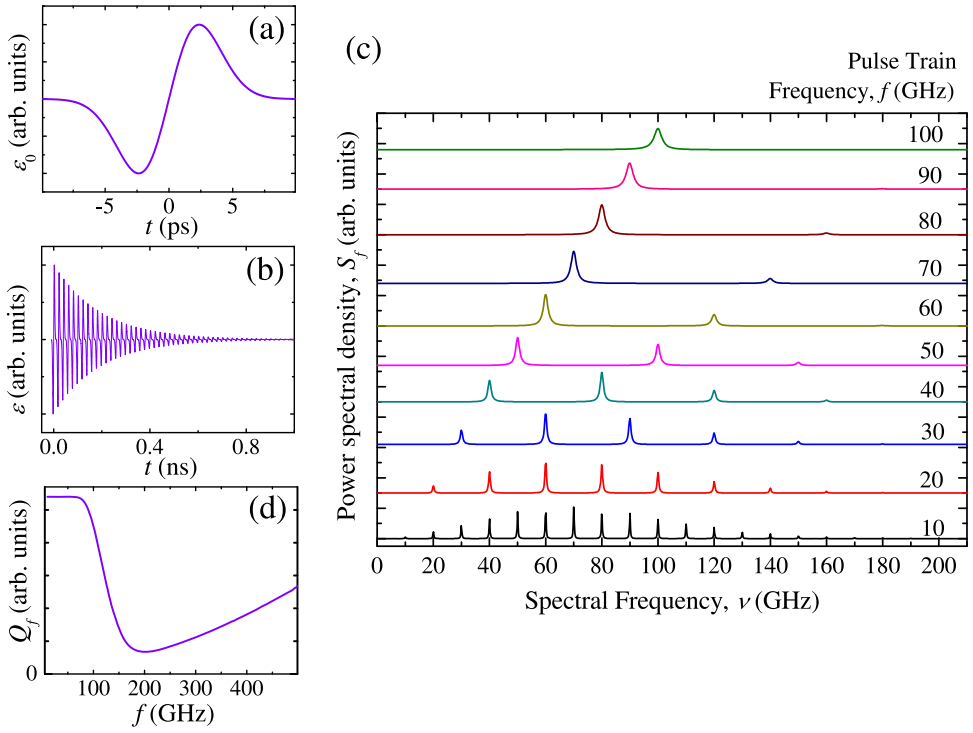

Figure 2. The simulation of the hypersonic excitations: (a) the temporal evolution of a single strain pulse, such as would be generated in a 30 nm Al film; (b) the train of picosecond strain pulses for $f = 50$ GHz; (c) the power spectra of the hypersonic excitation in the strain pulse train for a number of frequencies f; (d) the total elastic energy, Q_f in the hypersonic train as a function of the frequency f in the train. For simplicity the simulations do not include the mismatch between the Al film transducer and GaAs substrate.

for various train frequencies f obtained as fast Fourier transforms in a time window 5 ns which significantly exceeds the duration of the trains. It is seen that at low frequencies, $f \sim 10$ GHz, the spectrum possesses a number of spectral lines centred at frequencies $\nu = nf$, where $n = 1, 2, 3 \ldots$ is the harmonic number. For high

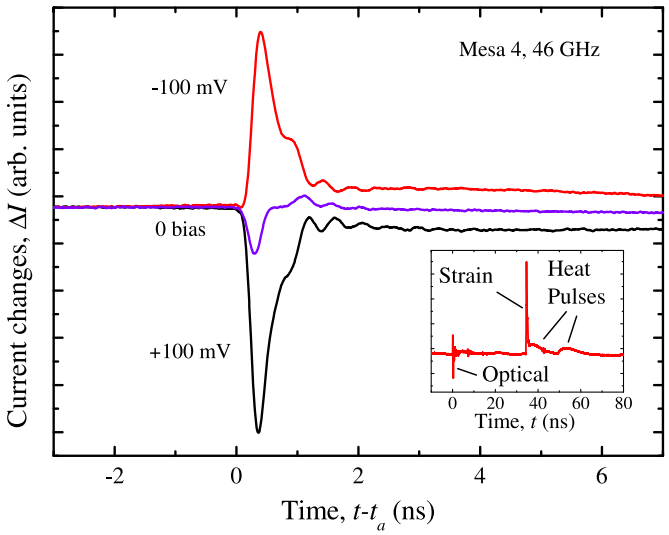

Figure 3. Temporal evolutions of the measured current for three values of bias V and $f = 46$ GHz; $t = t_a$ corresponds to the arrival time of the first strain pulse in the train to the SL. Inset shows the measured signal in the extended time interval where $t = 0$ corresponds to the optical excitation the Al film by the pump pulse.

$f > 60$ GHz, one spectral line with $n = 1$ dominates and in this range of f we may consider the hypersonic spectrum in the strain pulse train as essentially single harmonic with frequency $\nu = f$.

In the example shown in figure 2 (c) the intensity of the harmonic peak goes down at $f \sim 90$ GHz because individual strain pulses merge and interfere destructively due to their bipolar character (see the individual pulse in the figure 2 (a)). Further increase of f eventually leads to constructive interference of the individual strain pulses and in the limit of high $f \sim 1$ THz the train is modified to a single strain pulse with the amplitude equal to the sum of the strain amplitudes in the train. This behaviour is clearly demonstrated in figure 2 (d), which shows the dependence of the hypersonic energy in the strain pulse train on f, Q_f, integrated over the whole acoustic spectrum ($0 < \nu < 50$ THz): for $f < 90$ GHz, when individual strain pulses are not interfering, Q_f is constant; at $90 < f < 150$ GHz (destructive interference) Q_f decreases; and at $f > 150$ GHz Q_f increases with the increase of f due to constructive interference.

In the present work, the described experimental technique making use of strain pulse trains is employed to study the impact of harmonic hypersound on the transport properties of the SL. In the experiments, the injected strain pulse train propagates through the GaAs substrate and reaches the SL. The stationary dc current measured in the absence of strain, with an applied bias V is denoted I_0. The hypersonic-induced changes of the current in the SL, $\Delta I(t) = I(t) - I_0$ were measured using a 12.5 GHz bandwidth oscilloscope. The signal $\Delta I(t)$ is studied as a function of f, V, and the amplitude of the strain pulses in the train.

2.2. Experimental results

Figure 3 shows temporal traces $\Delta I(t)$ of the hypersonic induced changes of the current $I(t)$. The presented signals were detected in the studied SL (mesa M4) for the frequency $f = 46$ GHz. The traces are recorded for three values of the applied bias V. The signals possess a pulse arriving at a time, $t_a = 34.2$ ns, which is equal to the propagation time for longitudinal sound from the Al transducer to the SL through the GaAs substrate (see inset in figure 3, where the pulse corresponding to optical breakthrough is also shown). The strain pulse is followed by the heat pulses related to longitudinal and transverse ballistic incoherent phonons [43]. The signals detected for reasonably high V, but at $|V| < |V_t|$, show that $\Delta I(t) < 0$ for $V > 0$ and $\Delta I(t) > 0$ for $V < 0$. This means that the hypersonic waves induce a decrease of current in the SL. The $\Delta I(t)$ measured at $V = 0$ possess much smaller amplitude than $\Delta I(t)$ measured under bias, and depend on the particular mesa measured.

Figure 4 shows the traces $\Delta I(t)$ for several frequencies f of the excitation pulse train. These traces were all normalized to the same magnitude for clarity. For low frequencies, $f < 10$ GHz, the individual pulses in the train may be resolved and examples of this case are shown for $f = 5$ and 7.5 GHz (see two upper curves in figure 4). For the intermediate frequencies, $10 < f < 30$ GHz, the individual pulses are not resolved, but the mean duration $\bar{\tau}$ of the detected pulse $\Delta I(t)$ decreases with the increase of f. For high frequencies, $f > 40$ GHz, $\bar{\tau} \approx 500$ ps as characterized by the full width at half maximum and is independent of f. Such behaviour of the temporal evolution for $\Delta I(t)$ may be understood if we assume that hypersonic-induced changes of $\Delta I(t)$ occur only when the strain pulse train is propagating through the SL. Then the dependence of temporal shape of $\Delta I(t)$ on f can be

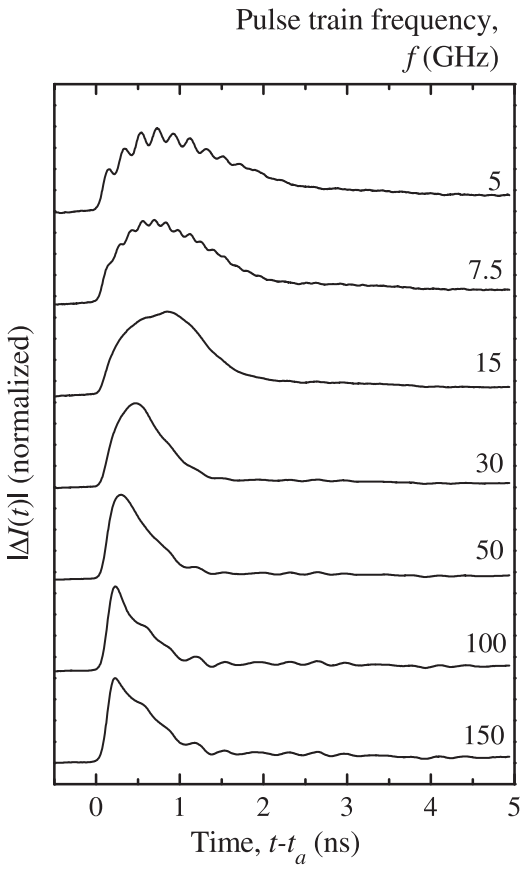

Figure 4. The temporal traces of the hypersonic induced current pulses measured at $V = 300$ mV in mesa M3 for various frequencies of the strain pulse train. These were all normalized to the same amplitude for clarity.

obtained qualitatively from temporal/spatial relations between the duration of the excitation pulse train and the total thickness of the studied SL. A single strain pulse propagates through the SL in forward and, after reflection from the open surface, reverse direction in a time $t_p = 2(L_{SL} + C)/s = 304$ ps, where $s = 5 \times 10^3 \mathrm{ms}^{-1}$ is the sound velocity and $L_{SL} + C = 760$ nm is the propagation path which includes the SL and top contact with the thicknesses $L_{SL} = 490$ nm and $C = 270$ nm respectively. In the low frequency limit, there is only one strain pulse travelling in the SL and the impact on the SL current from individual pulses in the train can be easily resolved. Alternatively, in the high-frequency limit ($f \gg 1/t_p$), when the spatial length of the whole strain pulse train is shorter than the SL's thickness, we may expect that the duration of the impact on the SL current is limited by the propagation time and thus $\sim t_p$. This simple explanation is consistent with the experimental observations presented in figure 4. Thus the dependence of the shapes of $\Delta I\,(t)$ on f confirms our assumption about the hypersonic impact on the carriers in the SL being the main origin of $\Delta I\,(t)$. A single polarity of $\Delta I\,(t)$ (positive or negative depending on the sign of V) excludes the strong contribution of hypersonic impacts on the contacts and interfaces of the device which are known to have bipolar temporal shape [44].

In further presentations of the experimental result we use the value, Δq, of the electrical charge transferred in the SL under the hypersonic impact:

$$\Delta q = \int_0^{t'} \Delta I\,(t)\,\mathrm{d}t, \tag{1}$$

where the upper limit, t', of the integral essentially exceeds the duration of the strain pulse train and its propagation time through the SL.

Figures 5 and 6 show the dependencies of Δq on bias V and optical excitation density J_0 of the train respectively. We limit our consideration to bias values $|V| < |V_t|$ when no charge domains are formed in the SL. In this regime we find that the temporal shape of $\Delta I\,(t)$ does not depend on J_0 and V. Figures 5 and 6 show the data for various mesas, the current–voltage curves of which are shown in figure 1(b). Remarkably figure 5 shows that with good approximation the dependencies of Δq on V are close to linear for all mesas and values of f. The dependencies of $\Delta I\,(t)$ on J_0 shown in log/log scale in figure 6 are mostly superlinear and close to square-law dependence, $\Delta q \sim J_0^2$ (compare with the solid and dashed lines which show the square and linear dependencies respectively). It is useful to mention that the values of J_0 used in our experiments correspond to strain

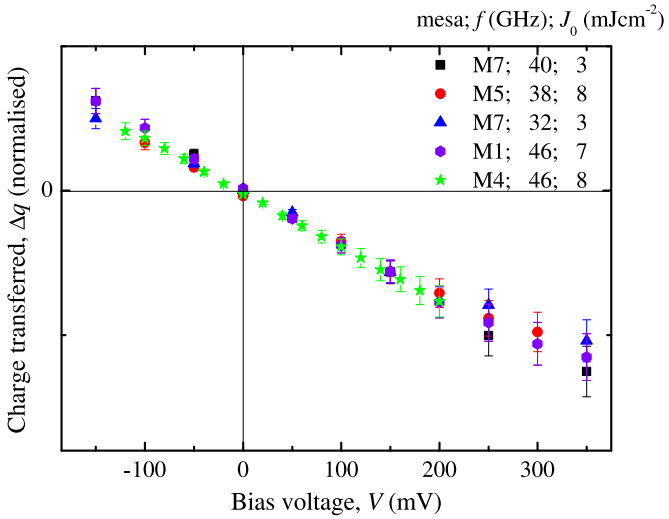

Figure 5. The total charge transferred through the superlattices in various mesas as a function of bias voltage. The large differences in magnitude between the different data sets makes comparison between them difficult. The curves were therefore all normalized to be of equal amplitude at V= 150 mV.

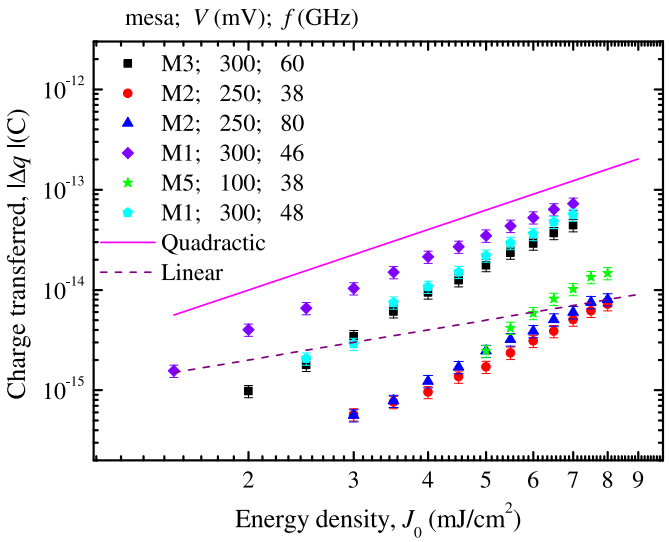

Figure 6. The charge transferred through the superlattices in various mesas as a function of the optical pump energy density on the Al film. Solid and dashed lines show quadratic and linear dependencies.

amplitudes in the train $\varepsilon < 10^{-4}$, [45]. At this value acoustic nonlinear effects are not strongly pronounced in the GaAs substrate used in our experiments [45–47]. Thus we must explain the observed nonlinearity of Δq on J_0 taking into account the mechanism of hypersonic-electrical transduction and not elastic nonlinearities.

3. Analysis and discussion

In the present section we discuss the experimental results presented in section 2. For this we present a theoretical model describing the hypersonic-electrical transformation in the SL, and use this model for the comparison between the experiment and theory (section 3.1). Finally, in section 3.2, we discuss the spectral efficiency of the hypersonic-electrical transformation in the SL analyzing the experimental and simulated dependencies of the hypersonic-induced changes of the SL current on the frequency in excitation train.

3.1. Theoretical model and comparison with experiment

In order to analyze the hypersonic-electric impact in the SL we follow an approach similar to that previously used to study the dc current in weakly coupled SLs under electromagnetic THz radiation [48, 49]. In a weakly

coupled SL, the vertical electron transport is due to sequential tunnelling through the potential barriers of the SL. It is assumed that the tunnelling events are independent, meaning that the electron tunnelling probability is affected by the energy $\hbar\omega$ of the excitation quantum, but is not sensitive to its phase. Then the action of a continuous harmonic acoustic wave at a given point in the SL can be represented by an effective electric field oscillating with the frequency of the hypersonic wave $\omega = 2\pi\nu$, and having the amplitude $\varepsilon D/(ed)$, where ε is strain amplitude in the acoustic wave, D is electron deformation potential, e is the electron charge, and d is the SL period. Thus, the joint action of the hypersonic wave and a dc bias V applied to the SL can be represented by an equivalent voltage $V_{ac}(t) = V + \varepsilon DL_{SL}\sin(\omega t)/(ed)$, where L_{SL} is the SL's length. In this case, the electrical current through the SL can be estimated as [49, 50]:

$$I(V) = \sum_{n=-\infty}^{+\infty} J_n^2(\alpha) I_0(V + n\hbar\omega/e). \tag{2}$$

Here, $J_n(.)$ is the Bessel function of the first kind, $\alpha = (\varepsilon DL_{SL})/(\hbar\omega d)$. For α sufficiently small the incremental current can be estimated as:

$$\Delta I(V) = I(V) - I_0(V) = \frac{1}{4}\left(\frac{\varepsilon DL_{SL}}{ed}\right)^2\left[\frac{I_0(V + \hbar\omega/e) - 2I_0(V) + I_0(V - \hbar\omega/e)}{(\hbar\omega/e)^2}\right]. \tag{3}$$

and, if the conductance of the SL varies slowly on the voltage scale $\hbar\omega/e$, equation (3) is reduced to

$$\Delta I(V) = \frac{1}{4}\left(\frac{\varepsilon DL_{SL}}{ed}\right)^2 \frac{d^2 I_0(V)}{dV^2}. \tag{4}$$

The estimation equation (4) is valid for the range of ω within which the expression in the square brackets in equation (3) is approximately equal to dI_0^2/dV^2. If one arbitrarily assumes that this approximate equality is held for $\hbar\omega/e$ which is at least an order of magnitude less than the bias V, then for V of the order 100 mV, the range of equation (4) validity extends up to $\omega \cong 500$ GHz.

In order to confirm the validity of this approach, we use the current–voltage characteristics $I_0(V)$ of the experimentally studied mesas and approximate the ascending part of the curve by a cubic polynomial which is a simple nonlinear approximation of the current–voltage characteristics of tunnel devices [51].

$$I_0(V) = aV + bV^3, \tag{5}$$

where a and b are the fitting parameters, which depend on the electrical properties of the quantum device. For instance, for mesa M3 the least-squares fitting of this polynomial with $a = 1.67 \times 10^{-2}$ S and $b = -7.1 \times 10^{-3}$ SV^{-2} to the experimental current–voltage curve gives an excellent agreement.

It is obvious that the strongly doped electrical contact regions will play an important role in redistribution of an electric field inside the device, hence their effect should also be taken into account in a self-consistent approach [52–54]. A detailed theoretical model including the effects of the device contacts is beyond the scope of this work. We adopt a much simplified approach to including the contact effects in the calculation of the magnitude of the device response to the acoustic impact by just replacing L_{SL} in equation (4) by the total length, L, of the device including SL and contact regions. Now, substituting equation (5) in equation (4) yields an analytical estimation of the incremental current

$$\Delta I(V) = \frac{3b}{2}\left(\frac{DL}{ed}\right)^2 \varepsilon^2 V. \tag{6}$$

Notably, the same equation can be obtained by substituting $V_{ac}(t) = V + \varepsilon DL\sin(\omega t)/(ed)$ into $I_0(V) = aV + bV^3$ and averaging the current I over the period $2\pi/\omega$.

The theoretical analysis of the hypersonic induced current changes described by the equations (5) and (6) predicts a linear dependence of $\Delta I(V)$ on V and a square-law dependence on strain amplitude, $\Delta I(V) \sim \varepsilon^2$. The experimental results presented in figures 5 and 6 show good agreement with these predictions. With good approximation, in most cases, $\Delta q \sim V$ (see figure 5) and $\Delta q \sim J_0^2 \sim \varepsilon^2$ (see figure 6). Minor discrepancies may be explained by the $I_0(V)$-curve needing a more sophisticated fit than the simple cubic polynomial, equation (5).

To provide more convincing evidence of the validity of the proposed theoretical model, we attempt a quantitative comparison of the absolute values of measured hypersonic-induced signals with $\Delta I(V)$ calculated by equation (6). As an example, we make the comparison for mesa M3, for which a good fit to the $I_0(V)$ curve can be obtained using equation (5) with $b = -7.1 \times 10^{-3}$ SV^{-2}. We choose the experimental signal $\Delta I(V)$ measured for $V = 300$ mV and $f = 60$ GHz for which the excitation may be considered with high accuracy as single harmonic. Then, for the example of $J_0 = 7$ mJ cm^{-2}, we obtain experimentally the maximal current $\Delta\bar{I} = \Delta q/\bar{\tau} = 8.7 \times 10^{-5}$A, where $\bar{\tau} = 530$ ps is the mean duration of $\Delta I(V)$. It is also important to note that the acoustic excitation used in the experiment is represented not by a continuous harmonic wave, but by an

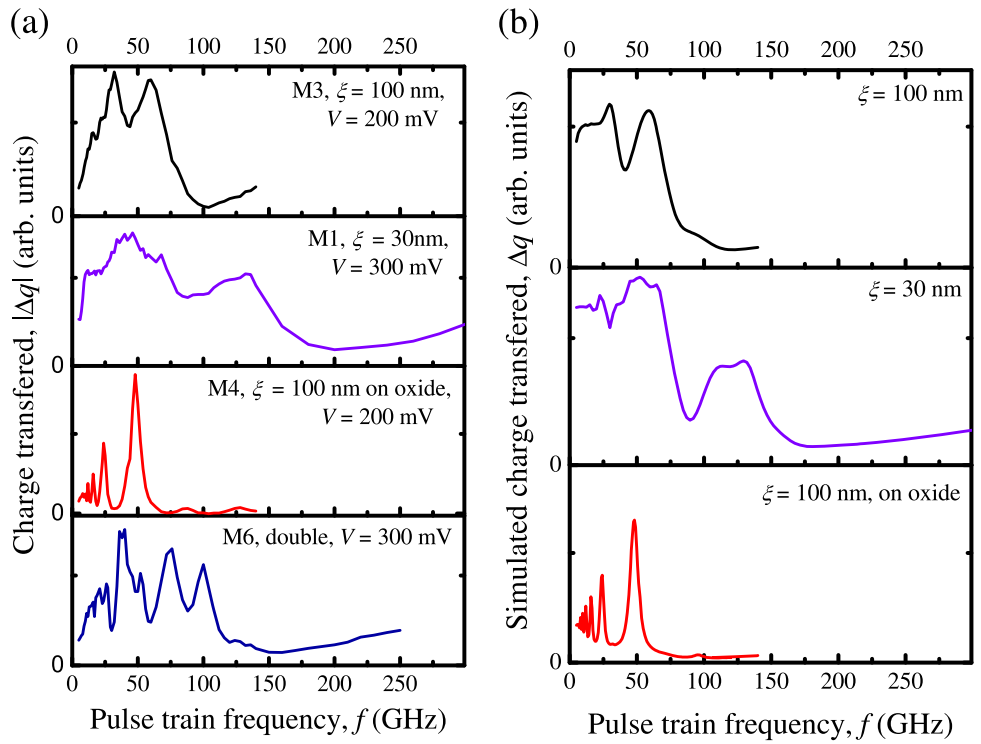

Figure 7. The measured (a) and simulated (b) transferred charge as a function of the strain pulse train frequency, *f*, for various Al films deposited on the GaAs substrate.

exponentially decaying pulse train (see figure 2(b)). However, the quality factor of the cavity used for this experiment is such that the decay of the acoustic excitation is not significant over the period of an acoustic wave. We estimate values for strain amplitude ε in the pulse train from the known fact that for individual strain pulses $\varepsilon \sim 10^{-4}$ for excitation density ~1 mJ cm^{-2} [45]. The energy J_1 of the first pulse in our experimental train is directly related to the total energy J_0 exiting the FP cavity as $J_1 = 0.11J_0$. Therefore, for $J_0 = 7$ mJ cm^{-2}, we get $\varepsilon = 7.7 \times 10^{-5}$, and, using the total length of the mesa including contact regions, $L = 1.3$ μm, then, within the framework of the simplification above, the theoretical estimation equation (6) gives the changes in the dc current $\Delta I = 3.2 \times 10^{-5}$A. This compares favourably with the value of the maximal incremental current measured experimentally, especially in view of the variability of the $I_0(V)$ fitting parameter b between different experimental runs.

3.2. Spectral characteristic of the hypersonic-electrical transformation

In this sub-section, we present the experimental results for the dependence of the detected signal Δq as a function of the frequency f of the strain pulse train. We make a qualitative comparison between these results and the theoretical model presented in the previous section and thus reach conclusions about the spectral sensitivity of the SL as a hypersonic-electrical transducer.

We present the dependencies $\Delta q(f)$ measured for a number of different Al films used as hypersonic generators. All the Al films were deposited on the surface of the sample at room temperature by thermal evaporation of Al wire. The thickness of the deposited films was controlled by a quartz crystal monitor during the evaporation and the nominal thicknesses were recorded. Figure 7 (a) shows the measured dependencies $\Delta q(f)$ and the nominal film thicknesses: mesa M3 was used to measure a 100 nm Al film; mesa M1 was used to measure a 30 nm Al film; mesa M4 was used to measure an 100 nm Al film deposited on the oxidized AlAs layer[3]; and mesa M6 was used to measure a 60 nm Al film deposited on top of an oxidized 50 nm Al film (after keeping the sample with the 50 nm film in the air for approximately 4 hours).

The measured dependencies $\Delta q(f)$ are very different for different Al films. All the curves show spectral peaks, but the number of the peaks, their width and the contrast relative to the background are very different. Mesa M3 shows two broad peaks at approximately 59 and 32 GHz and a deep minimum around 100 GHz. In

[3] An etch was performed to remove an unnecessary structure from the reverse of the sample, which is thought to have stopped slightly short resulting in an AlAs layer being exposed rather than the intended GaAs layer. The oxidization and subsequent roughening of this AlAs layer is thought to be the cause of poor adhesion of this film.

mesa M1 the peaks are observed at approximately 134 and 45 GHz. It is interesting that mesas M4 and M6 show a number of narrow and well-defined peaks.

To understand the measured dependencies $\Delta q\,(f)$ we at first calculate the hypersonic power spectra $S_f\,(\nu)$ of the strain pulse trains, taking into account the multiple reflections of hypersonic waves in the Al film. We describe the form of a single strain pulse $\varepsilon_0\,(t)$ injected into GaAs substrate with the following equation:

$$\varepsilon_0\,(t) \sim \sum_{j=0}^{+\infty}(-R)^j\left(t-\frac{2j\xi}{s_{\mathrm{Al}}}\right)\exp\left[-\frac{1}{\tau_{\mathrm{Al}}^2}\left(t-\frac{2j\xi}{s_{\mathrm{Al}}}\right)^2\right], \tag{7}$$

where R is the reflection coefficient for longitudinal sound at the interface between the Al film and the GaAs, s_{Al} is the speed of longitudinal sound in the Al film, ξ is the thickness of the film and τ_{Al} is a parameter used to adjust the width of the bipolar pulse for different film thicknesses. Using the theoretically predicted square-law dependence of Δq on strain for the harmonic hypersonic wave, i.e. $\Delta q \sim \varepsilon^2$, and that Δq is independent of f, means that the signal will be proportional to the total hypersonic energy Q_f of the strain pulse train:

$$\Delta q \sim Q_f = \int_0^{\infty} S_f\,(\nu)\,\mathrm{d}\nu \tag{8}$$

The calculated dependencies Q_f are shown in figure 7 (b). To perform these simulations we used the thickness of the Al film ξ, reflection coefficients R at the Al/GaAs interface, and characteristic duration τ_{Al} of the individual strain pulse in the train as fitting parameters. For mesa M3 we find an excellent agreement with the experiment (compare upper curves on figures 7 (a) and (b)) using $\xi_1 = 78$ nm, $\tau_{\mathrm{Al1}} = 5.5$ ps and $R_1 = 0.18$ which are consistent with the nominal thickness 100 nm, and R obtained from the acoustic mismatch theory at the Al/GaAs interface. For the mesa M1 a good agreement with the experiment is obtained (compare the second curves down on figures 7 (a) and (b)) by using the parameters $\xi_2 = 43$ nm, $\tau_{\mathrm{Al2}} = 3.4$ ps and $R_2 = 0.43$. The value of R_2 is twice higher than the value obtained from acoustic mismatch. For mesa M4 the agreement with the experimental curve is obtained using the values $\xi_3 = 66$ nm, $\tau_{\mathrm{Al3}} = 6.4$ ps and $R_3 = 0.45$. For this sample better agreement with the experimental situation was obtained when no phase change was included when the strain pulse is reflected at the Al/GaAs interface. The well-defined peaks seen in mesa M4 are thought to originate from the lack of phase change at the Al/GaAs interface. No fitting was attempted for mesa M6 due to the increase in the number of fitting parameters required in the case of the double Al film. The cases of mesas M4 and M6, which show sharp peaks in the dependencies $\Delta q\,(f)$ (see figure 7 (a)), are of particular interest because the results cannot be explained by acoustic mismatch theory. However these and similar observations reported earlier by other groups [55–58], stay beyond the present paper and demand more detailed studies.

From the obtained agreement between the experiment and theory, we may conclude that the approximation made in equation (8) is valid for a wide range of acoustic frequencies, f. We think that the minor difference between theory and experiment is due to the harmonic approximation of the theoretical approach while the spectrum $S_f\,(\nu)$, especially at low f, possesses many sub-harmonics and the maximum intensity does not correspond to $\nu = f$. In the case of broad spectrum excitation, the theoretical approach should probably be modified in accordance with the similar considerations for electromagnetic waves [50]. However, the results confirm the theoretical prediction of a flat spectral sensitivity of hypersonic-electrical transformation in the studied frequency range.

4. Conclusions and outlook for the future

In conclusion, we have investigated the effects of a hypersonic pulse train on charge transport properties of weakly coupled n-doped SL devices. The experiments show that the time evolution of the electrical response is governed by the repetition rate, f, of the strain pulses in the train and its time of propagation through the superlattice. The measured signals clearly show rectification of the hypersonic excitation, which is explained by a theoretical model based on the same principles as for rectification of electromagnetic waves. Both the amplitude of current pulses induced by hypersonic stimuli and the total transferred charge increase superlinearly with the growth of strain amplitude in the hypersonic wave packet. These effects can be explained by the nonlinearity of the current voltage characteristics in the tunnelling devices. Our theoretical analysis suggests a flat spectral response of the rectified current to the hypersonic frequency. This is confirmed by the experiments performed using generated hypersonic wavepackets with various spectral characteristics.

The experiments and theoretical analysis indicate the possibility for hypersonic to electromagnetic conversion in the SL device. Using hypersonic wavepackets consisting of trains of picosecond strain pulses injected into periodic tunnelling devices shows the prospective for exploring high-frequency (GHz and sub-THz) acoustic harmonic excitations in microwave and ultrafast electronics. In the present work, we have shown that the measured current pulses reflect the dc response of the SLs to the hypersonic wavepackets. However, the ac component should also be present, as appears in SL-based detectors of microwave radiation [59]. In fact the

oscillating current is detected at GHz frequencies within the oscilloscope bandwidth. However, for detection of higher frequencies more advanced THz radiation detection techniques, e.g. electro-optic sampling, should be used.

The harmonic hypersonic impact on the electrical properties of the SLs is not limited by the transformation of acoustic wave into an electrical response. The technique opens the possibility to search for the hypersonic control of high frequency electron transport [31, 32]. Other possible applications concern various parametric effects in THz electronics, for example: a superlattice with its electron states modulated by harmonic hypersonic waves may control the reflection of THz radiation and emission in quantum cascade lasers.

Acknowledgments

We acknowledge EPSRC and US Army RDECOM Forward Element CommandAtlantic for financial support under grant numbers: EP/M016161/1, EP/M016099/1 and W911NF-14-1-0586 respectively. We are thankful to Prof T M Fromhold and Dr B A Glavin for helpful discussions.

References

[1] Esaki L and Tsu R 1970 Superlattice and negative diferential conductivity in semiconductors *IBM J. Res. Dev.* **14** 61–65
[2] Hofbeck K *et al* 1996 High-frequency self-sustained current oscillation in an Esaki–Tsu superlattice monitored via microwave emission *Phys. Lett.* A **218** 349–53
[3] Schomburg E, Scheuerer R, Brandl S, Renk K F, Pavel'ev D G, Koschurinov Y, Ustinov V, Zhukov A, Kovsh A and Kop'ev P S 1999 InGaAs/InAlAs superlattice oscillator at 147 GHz *Electron. Lett.* **35** 1491–2
[4] Schomburg E, Henini M, Chamberlain J M, Steenson D P, Brandl S, Hofbeck K, Renk K F and Wegscheider W 1999 Self-sustained current oscillation above 100 GHz in a GaAs/AlAs superlattice *Appl. Phys. Lett.* **74** 2179–81
[5] Sankin I, Andrianov A V, Zakharin A O and Petrov A G 2011 Terahertz radiation induced by the Wannier–Stark localization of electrons in a natural silicon carbide superlattice *J. Exp. Theor. Phys. Lett.* **94** 362–5
[6] Eisele H, Farrer I, Linfield E H and Ritchie D A 2008 High-performance millimeter-wave superlattice electronic devices *Appl. Phys. Lett.* **93** 182105
[7] Ktitorov S A, Simin G S and Sindalovskü V Ya 1972 Bragg reflections and high-frequency conducticty of an electronic solid-state plasma *Sov. Phys.—Solid State* **13** 1872
[8] Shimada Y, Hirakawa K, Odnoblioudov M and Chao K A 2003 Terahertz conductivity and possible Bloch gain in semiconductor superlattices *Phys. Rev. Lett.* **90** 046806
[9] Terazzi R, Gresch T, Giovannini M, Hoyler N, Sekine N and Faist J 2007 Bloch gain in quantum cascade lasers *Nat. Phys.* **3** 329–33
[10] Hyart T, Alekseev K N and Thuneberg E V 2008 Bloch gain in dc–ac-driven semiconductor superlattices in the absence of electric domains *Phys. Rev.* B **77** 165330
[11] Capasso F, Gmachl C, Sivco D L and Cho A Y 2002 Quantum cascade lasers *Phys. Today* **55** 34–40
[12] Faist J, Capasso F, Sivco D L, Sirtori C, Hutchinson A L and Cho A Y 1994 Quantum cascade laser *Science* **264** 553–6
[13] Hyart T, Alexeeva N V, Leppänen A and Alekseev K N 2006 Terahertz parametric gain in semiconductor superlattices in the absence of electric domains *Appl. Phys. Lett.* **89** 132105
[14] Renk K F, Rogl A and Stahl B I 2007 Semiconductor-superlattice parametric oscillator for generation of sub-terahertz and terahertz waves *J. Lumin.* **125** 252–8
[15] Bomze Y, Hey R, Grahn H T and Teitsworth S W 2012 Noise-induced current switching in semiconductor superlattices: obsevation of nonexponential kinetics in a high-dimensional system *Phys. Rev. Lett.* **109** 026801
[16] Huang Y, Qin H, Li W, Lu S, Dong J, Grahn H T and Zhang Y 2014 Experimental evidence for coherence resonance in a noise-driven GaAs/AlAs superlattice *Europhys. Lett.* **105** 47005
[17] Hizanidis J, Balanov A, Amann A and Schöll E 2006 Noise-induced front motion: signature of a global bifurcation *Phys. Rev. Lett.* **96** 244104
[18] Zhang Y, Kastrup J, Klann R, Ploog K H and Grahn H T 1996 Synchronization and chaos induced by resonant tunneling in GaAs/AlAs superlattices *Phys. Rev. Lett.* **77** 3001–4
[19] Aoki H and Kaneko K 2013 Slow stochastic switching by collective chaos of fast elements *Phys. Rev. Lett.* **111** 144102
[20] Hramov A E *et al* 2014 Subterahertz chaos generation by coupling a superlattice to a linear resonator *Phys. Rev. Lett.* **112** 116603
[21] Alvaro M, Carretero M and Bonilla L L 2014 Noise-enhanced spontaeous chaos in semiconductor superlattices at room temperature *Europhys. Lett.* **107** 37002
[22] Huang Y, Li W, Ma W, Qin H, Grahn H T and Zhang Y 2013 Spontaneous quasi-periodic current self-oscillations in a weakly coupled GaAs/(Al,Ga)As superlattice at room temperature *Appl. Phys. Lett.* **102** 242107
[23] Renk K F, Rogl A, Stahl B I, Meier A, Koschurinov Yu I, Pavel'ev D G, Ustinov V, Zhukov A, Maleev N and Vasilyev A 2006 Semiconductor-superlattice frequency mixer for detection of submillimeter waves *Int. J. Infrared Millim. Waves* **27** 373–80
[24] Endres C P, Lewen F, Giesen T F, Schlemmer S, Paveliev D G, Koschurinov Y I, Ustinov V M and Zhukov A E 2007 Application of superlattice multipliers for high-resolution terahertz spectroscopy *Rev. Sci. Instrum.* **78** 043106
[25] Li W, Reidler I, Avaid Y, Huang Y, Song H, Zhang Y, Rosenbluh M and Kanter I 2013 Fast physical random-number generation based on room-temperature chaotic oscillaitons in weakly coupled superlattices *Phys. Rev. Lett.* **111** 044102
[26] Cavill S A, Challis L J, Kent A J, Ouali F F, Akimov A V and Henini M 2002 Acoustic phonon-assisted tunneling in GaAs/AlAs superlattices *Phys. Rev.* B **66** 235320
[27] Glavin B A, Kochelap V A and Linnik T L 1999 Generation of high-frequency coherent acoustic phonons in a weakly coupled superlattice *Appl. Phys. Lett.* **74** 3525–7
[28] Kent A J, Kini R N, Stanton N M, Henini M, Glavin B A, Kochelap V A and Linnik T L 2006 Acoustic phonon emission from a weakly coupled superlattice under vertical electron transport: observation of phonon resonance *Phys. Rev. Lett.* **96** 215504

[29] Poyser C L, Akimov A V, Campion R P and Kent A J 2015 Coherent phonon optics in a chip with an electrically controlled active device *Sci. Rep.* **5** 8279
[30] Maryam W, Akimov A V, Campion R P and Kent A J 2013 Dynamics of a vertical cavity quantum cascade phonon laser structure *Nat. Commun.* **4** 2184
[31] Greenaway M T, Balanov A G, Fowler D, Kent A J and Fromhold T M 2009 Using sound to generate ultra-high-frequency electron dynamics in superlattices *Microelectron. J.* **40** 725–7
[32] Greenaway M T, Balanov A G, Fowler D, Kent A J and Fromhold T M 2010 Using acoustic waves to induce high-frequency current oscillations in superlattices *Phys. Rev.* B **81** 235313
[33] Bartels A, Dekorsy T and Kurz H 1999 Coherent zone-folded longitudinal acoustic phonons in semiconductor superlattices: excitation and detection *Phys. Rev. Lett.* **82** 1044–7
[34] Pascual-Winter M F, Fainstein A, Jusserand B, Perrin B and Lemaître A 2012 Spectral reponses of phonon optical generation and detection in superlattices *Phys. Rev.* B **85** 235443
[35] Hawker P, Kent A J, Challis L J, Bartels A, Dekorsy T, Kurz H and Köhler K 2000 Observation of coherent zone-folded acoustic phonons generated by Raman scattering in a superlattice *Appl. Phys. Lett.* **77** 3209–11
[36] Sun C-K, Liang J-C and Yu X-Y 2000 Coherent acoustic phonon oscillations in semiconductor multiple quantum wells with piezoelectric fields *Phys. Rev. Lett.* **84** 179
[37] Thomsen C, Grahn H T, Maris H J and Tauc J 1986 Surface generation and detection of phonons by picosecond light pulses *Phys. Rev.* B **34** 4129–38
[38] Pezeril T, Klieber C, Andrieu S and Nelson K A 2009 Optical generation of gigahertz-frequency shear acoustic waves in liquid glycerol *Phys. Rev. Lett.* **102** 107402
[39] Klieber C, Péronne E, Katayama K, Choi J, Yamaguchi M, Pezeril T and Nelson K A 2011 Narrow-band acoustic attenuation measurements in vitreous silica at frequencies between 20 and 400 GHz *Appl. Phys. Lett.* **98** 211908
[40] Bonilla L L and Grahn H T 2005 Non-linear dynamics of semiconductor superlattices *Rep. Prog. Phys.* **68** 577–683
[41] Beardsley R P, Campion R P, Glavin B A and Kent A J 2011 A GaAs/AlAs superlattice as an electrically pumped THz acoustic phonon amplifier *New J. Phys.* **13** 073007
[42] Akimov A V, Scherbakov A V, Yakovlev D R, Foxon C T and Bayer M 2006 Ultra-fast band-gap shift induced by a strain pulse in semiconductor heterostructures *Phys. Rev. Lett.* **97** 037401
[43] von Gutfield R J 1968 Heat pulse transmission *Physical Acoustics: Principles and Methods* vol 5, ed W Masson (New York: Academic) p 233
[44] Moss D M, Akimov A V, Glavin B A, Henini M and Kent A J 2011 Ultrafast strain-induced current in a GaAs Schottky diode *Phys. Rev. Lett.* **106** 066602
[45] Scherbakov A V, van Capel P J S, Akimov A V, Dijkhuis J I, Yakovlev D R, Berstermann T and Bayer M 2007 Chirping of an optical transition by an ultrafast acoustic soliton train in a semiconductor quantum well *Phys. Rev. Lett.* **99** 057402
[46] Péronne E and Perrin B 2006 Generation and detection of acoustic solitons in crystalline slabs by laser ultrasonics *Ultrasonics* **44** e1203–e1207
[47] Hao H-Y and Maris H J 2001 Experiments with acoustic solitons in crystalline solids *Phys. Rev.* B **64** 064302
[48] Keay B J, Zeuner S, Allen S J Jr, Maranowski K D, Gossard A C, Bhattacharya U and Rodwell M J W 1995 Dynamic localization, absolute negative conductance, and stimulated, multiphoton emission in sequential resonant tunneling semiconductor superlattices *Phys. Rev. Lett.* **75** 4102
[49] Wacker A and Jauho A-P 1997 Transport in a weakly-coupled superlattice: a quantitative approach for photon-assisted tunneling *Phys. Status Solidi* b **204** 73–76
[50] Tucker J R 1979 Quantum limited detection in tunnel junction mixers *IEEE J. Quantum Electron.* **15** 1234–58
[51] Chow W F 1964 *Principles of Tunnel Diode Circuits* (New York: Wiley)
[52] Greenaway M T, Balanov A G and Fromhold T M 2012 Controlling charge domain dynamics in superlattices *Nonlinear Laser Dynamics: From Quatum Dots to Crytography* vol 5, ed K Lüdge (Weinheim: Wiley)
[53] Balanov A G, Greenaway M T, Koronovskii A A, Moskalenko O I, Selskii A O, Fromhold T M and Khramov A E 2012 The effect of temperature on the nonlinear dynamics of charge in a semiconductor superlattice in the presence of a magnetic field *J. Exp. Theor. Phys.* **114** 836–40
[54] Maksimenko V A, Makarov V V, Koronovskii A A, Alekseev K N, Balanov A G and Hramov A E 2015 The effect of collector doping on the high-frequency generation in strongly coupled semiconductor superlattice *Europhys. Lett.* **109** 47007
[55] Tas G, Loomis J J, Maris H J, Bailes A A and Seiberling L E 1998 Picosecond ultrasonics study of the modification of interfacial bonding by ion implantation *Appl. Phys. Lett.* **72** 2235–7
[56] Clemens B M and Eesley G L 1988 Relationship between interfacial strain and the elastic response of multilayer metal films *Phys. Rev. Lett.* **61** 2356–9
[57] Grahn H T, Maris H J and Tauc J 1989 Picosecond Ultrasonics *IEEE J. Quantum Electron.* **25** 2562–8
[58] Rossignol C, Perrin B, Bonello B, Djemia P, Moch P and Hurdequint H 2004 Elastic properties of ultrathin permalloy/alumina multilayer films using picosecond ultrasonics and Brillouin light scattering *Phys. Rev.* B **70** 094102
[59] Platero G and Aguado R 2004 Photon-assisted transport in semiconductor nanostructures *Phys. Rep.* **395** 1–157